Mechanistic and Structural Studies of Electron-Deficient Quinoline Triosmium Clusters

Edgar Arcia, Douglas S. Kolwaite, and Edward Rosenberg*

Department of Chemistry, The University of Montana, Missoula, Montana 59812

Kenneth Hardcastle,* Joana Ciurash, and Ricardo Duque

Department of Chemistry, California State University, Northridge, Northridge, California 91330

Roberto Gobetto, Luciano Milone,* Domenico Osella, Mauro Botta, Walter Dastrú, and Alessandra Viale

Dipartimento di Chimica IFM, Universitá di Torino, 10125 Turin, Italy

Ian Fiedler

J. Heyrovsky Institute of Physical Chemistry, Academy of Sciences of the Czech Republic, Dolejskova 3, 18223, Prague, Czech Republic

Received July 7, 1997

Deuterium-labeling experiments on the sequential reactions of the previously reported electron-deficient complexes $Os_3(CO)_9(\mu_3\text{-}\eta^2\text{-}C_9H_4NRR')(\mu\text{-}H)$(R = R′ = H, **1a**; R = 4-Me, R′ = H, **1b**; R = H, R′ = 6-CH_3, **1c**) with X^-/X^+ (X = H or D) reveal that initial attack of H^- is at the 5-position of the quinoline ring and that the reduction of the C(5)−C(6) double bond to yield $Os_3(CO)_9(\mu_3\text{-}\eta^3\text{-}C_9H_6RR'N)(\mu\text{-}H)$ (**2a**−**c**) is not stereoselective. Related experiments with **2a**−**c** reveal that hydride attack at the 7-position is followed by protonation at the metal core to yield $Os_3(CO)_9(\mu_3\text{-}\eta^2\text{-}C_9H_7RR'N)(\mu\text{-}H)_2$ (**3a**−**c**). The conversion of **2a** to **3a** is also achieved by reaction with H_2 at 75 °C and 100 psi. When this reaction is carried out with excess D_2, deuterium incorporation is observed at C(7) and at the metal core, suggesting a concerted, irreversible hydrogen addition or a radical chain reaction. The related 46-electron cluster $Os_3(CO)_9(\mu_3\text{-}\eta^2\text{-}C_9H_8N)(\mu\text{-}H)$ (**5**) containing a C═N bond in a partially reduced heterocyclic ring, as well as the three-center two-electron bond at C(8), undergoes H^- attack at C(2) and not at C(5), as for **1a**−**c**, followed by protonation at the metal core to yield $Os_3(CO)_9(\mu_3\text{-}\eta^2\text{-}C_9H_9N)(\mu\text{-}H)_2$ (**4**). Photolysis or thermolysis of the previously reported $Os_3(CO)_9(\mu\text{-}\eta^2\text{-}(4\text{-Me})C_9H_5N)(\mu\text{-}H)(P(OEt)_3)$ (**6b**) does not yield the phosphite-substituted 46-electron clusters related to **1a**−**c** but leads only to nonspecific decomposition. Partially selective incorporation of ^{13}CO into **1a**−**c** is observed to yield the corresponding decacarbonyl derivatives, and the pattern of ^{13}CO incorporation helps to elucidate the interconversion of the nona- and decacarbonyl derivatives. The electrochemical behavior of **1a**, the dynamical behavior of **2b**, and the solid-state structures of **2b**, **3a**, **5**, and **6b** are reported.

Introduction

The study of the interaction of the quinoline ring system with mono- and polynuclear metal centers has received considerable attention in recent years in an attempt to model the heterogeneously catalyzed hydrodenitrification (HDN) of this nitrogen heterocycle.[1−6] Homogeneous model systems have shown that the first stage of hydrogenation is the reduction of the heterocyclic ring,[4] as indicated from product evolution studies in the heterogeneously catalyzed system.[1−3] We have subsequently studied the reactions of both quinoline[7] and tetrahydroquinoline[8] with the lightly stabilized cluster $Os_3(CO)_{10}(CH_3CN)_2$. The reaction with quinoline yields the novel 46-electron clusters $Os_3(CO)_9(\mu_3\text{-}\eta^2\text{-}C_9H_4RR'N)(\mu\text{-}H)$ (R = R′ = H **1a**; R = 4-Me, R′ = H, **1b**; R = H, R′ = 6-CH_3, **1c**) after thermolysis or photolysis

(1) Gates, B. C. *Catalytic Chemistry;* Wiley: New York, 1992; Chapter 6.
(2) Vivier, L.; D'Arau, O.-P.; Perot, G.; Kasztelan, S. *Prepr.—Am. Chem. Soc., Div. Pet. Chem.* **1992**, *37*, 710 and references therein.
(3) Ramirez, M. M.; Galaraga, E.; Pimentel, M. *Prepr.—Am. Chem. Soc., Div. Pet. Chem.* **1993**, *38*, 700.
(4) (a) Baralt, E.; Smith, S. J.; Hurwitz, J.; Horvath, I. T.; Fish, R. H. *J. Am. Chem. Soc.* **1992**, *114*, 5187. (b) Fish, R. H. *Aspects of Homogeneous Catalysis*; Ugo, R., Ed.; Kluwer Academic Publishers: The Netherlands, 1990; p 65. (c) Laine, R. M. *New J. Chem.* **1987**, *11*, 543.
(5) (a) Gray, S. D.; Smith, D. P.; Bruck, M. A.; Wigley, D. E. *J. Am. Chem. Soc.* **1992**, *114*, 5462. (b) Gray, S. D.; Fox, P. A.; Kingsborough, M. S.; Bruck, M. S.; Wigley, D. E. *Prepr.—Am. Chem. Soc., Div. Pet. Chem.* **1993**, *38*, 706.
(6) (a) Fish, R. H.; Kim, T. J.; Stewart, J. L.; Bushweller, J. H.; Rosen, R. K.; Dupon, J. W. *Organometallics* **1986**, *5*, 2193. (b) Eisenstadt, A.; Giandomenico, C. M.; Frederick, M. F.; Laine, R. M. *Organometallics* **1985**, *4*, 2033.

S0276-7333(97)00569-4 CCC: $15.00
Publication on Web 01/07/1998

of the initially formed decacarbonyls (eq 1). These

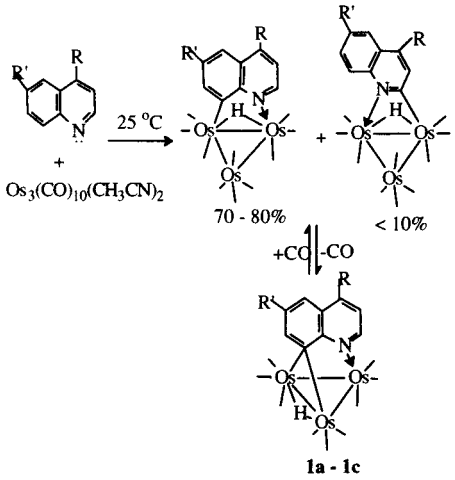

(1)

complexes undergo stoichiometric reduction at the carbocyclic ring on treatment with H^-/H^+ to give the 48-electron, σ-π-vinyl complexes $Os_3(CO)_9(\mu_3$-η^3-$C_9H_6RR'N)(\mu$-H) (**2a**−**c**, eq 2). A second round of H^-/H^+ leads to

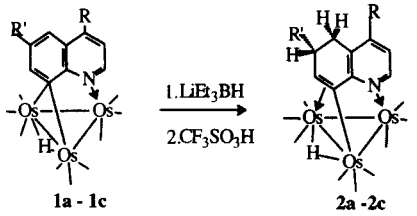

(2)

the complete reduction of the carbocyclic ring and the formation of the dihydrido clusters $Os_3(CO)_9(\mu_3$-η^2-C_9H_7-$RR'N)(\mu$-$H)_2$ (**3a**−**c**, eq 3).[7] These reactions represent

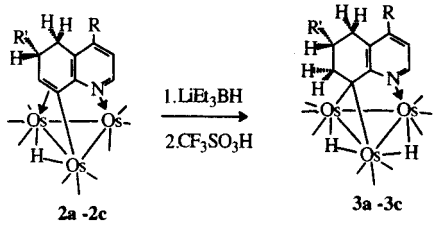

(3)

the first examples of selective reduction of the carbocyclic ring in quinoline, although studies of the catalytic system suggest that the initial reduction of this ring is a secondary pathway to HDN.[1]

In our previous studies of the reactivity of the tetrahydroquinoline complexes of triosmium clusters, we found that the initially formed tautomeric products $Os_3(CO)_9(\mu_3$-η^2-$C_9H_9N)(\mu$-$H)_2$ (**4a** and **4b**) dehydrogenate to a 46-electron green complex $Os_3(CO)_9(\mu_3$-η^2-$C_9H_8N)(\mu$-H) (**5**, eq 4).[8] The formation of this complex raises the question as to whether attack by hydride on **5** would be at the 5- or the 2-position of the quinoline ring.

We report here the results of deuterium-labeling studies which elucidate the reduction pathways of **1**, **2**, and **5** as well as some further studies on the fundamental properties of these complexes including the selective incorporation of ^{13}CO into **1**, the dynamics of **2**, and the electrochemical behavior of **1**. We also report the solid-state structures of **2b**, **3a**, and **5** and of the phosphite derivative of **1b**, $Os_3(CO)_9(\mu$-η^2-(4-Me)$C_9H_5N)(\mu$-H)P-$(OEt)_3$ (**6b**).

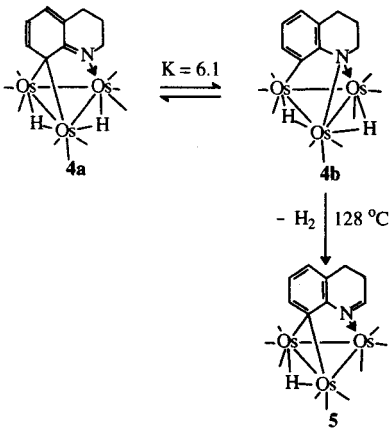

(4)

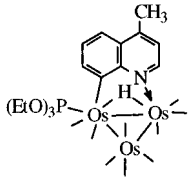

Results and Discussion

Deuterium-Labeling Studies of the Reduction of 1, 2, and 5. The reaction of D^-/D^+ with complex **1c** gave *cis* and *trans* isomers **2c**-d_2 (Scheme 1). The ^1H NMR of **2c** shows a multiplet at 2.17 ppm (H(6)). This multiplet is not evident in the ^1H NMR of **2c**-d_2, demonstrating that deuterium incorporation has occurred at the C(6) position of the carbocyclic ring. The ^1H NMR of **2c** shows a multiplet at 2.45 ppm for CH_2-(5), while in the ^1H NMR of **2c**-d_2, two singlets (2.41 and 2.54 ppm) are observed that are assignable to the *cis* and *trans* isomers. When D^-/H^+ is reacted with **1c** to give **2c**-*dh*, the multiplet at 2.17 ppm for H(6) is evident and has a relative intensity equal to that of the single protons in the aromatic region of the spectrum. The multiplet at 2.45 ppm in the ^1H NMR of **2c** is now two doublets at 2.52 ppm (J_{H-H} = 11.2 Hz (*trans*)) and 2.41 (J_{H-H} = 4.4 Hz (*cis*)). The relative intensity of the two *cis* and *trans* doublets is 1:1, indicating that there is no stereospecificity during protonation at the C(6) position (Scheme 1). This is likely due to the small size of the hydride and the proton. Studies with larger nucleophiles and electrophiles currently underway in our laboratory reveal that protonation can yield only the *cis* isomer after nucleophilic attack with carbanions and quenching with acid.[9]

Our initial studies on the second stage of the reduction (i.e., reduction of the C(7)−C(8) double bond) were not conclusive as to the site of the initial nucleophilic attack.[7] Studies using labeled hydride and proton donors show that the site of nucleophilic attack is regioselective at the C(7) position of the carbocyclic ring

(7) Kabir, S. E.; Kolwaite, D. S.; Rosenberg, E.; Hardcastle, K.; Cresswell, W.; Grindstaff, J. *Organometallics* **1995**, *14*, 3611 and references therein.

(8) Kabir, S. E.; Kolwaite, D. S.; Rosenberg, E.; Scott, L. G.; McPhillips, T.; Duque, R.; Day, M.; Hardcastle, K. I. *Organometallics* **1996**, *15*, 1979.

(9) Bergman, B.; Rosenberg, E.; Hardcastle, K. I.; Ciurash, J.; Duque, R. Manuscript in preparation.

Scheme 1

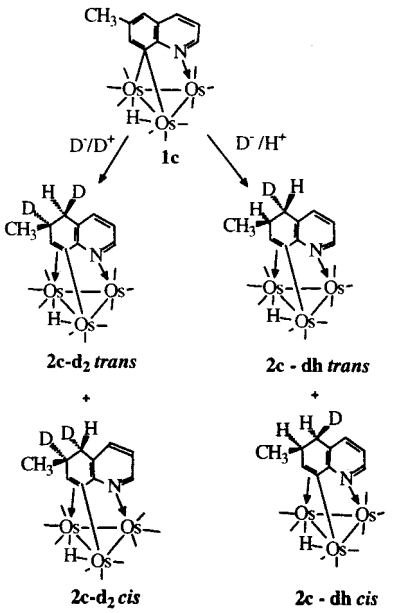

Scheme 2

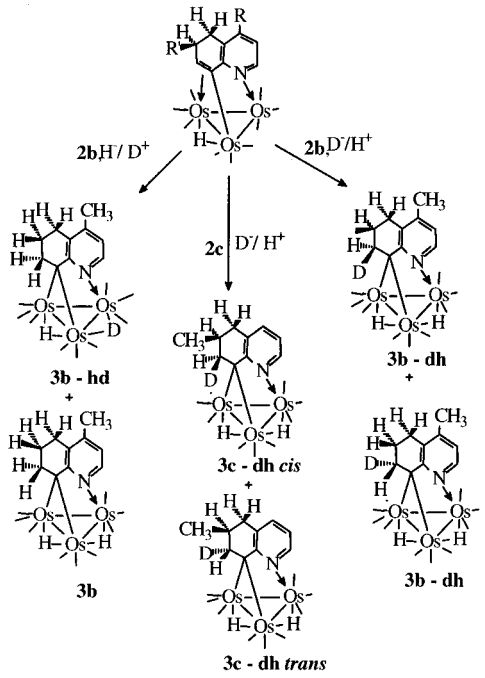

(Scheme 2). When compound **2b** is treated with H^-/D^+ to form **3b**-*hd*, the chemical shifts and peak multiplicities of the aromatic and aliphatic region of the ^1H NMR of **3b**-*hd* are consistent with the undeuterated form of the quinoline ring in **3b**. Changes are observed in the hydride region of the spectrum. A set of singlets are observed at −13.98 and −13.85 ppm and a set of doublets at −13.98 and −13.86 ppm in a ratio of 4:1. The observation of the two doublets indicates that some exchange of protons for deuterium at the hydride positions has taken place. It is possible that this takes place during chromatographic workup, but we see no evidence of this in any of our other labeling experiments. Another possibility is exchange with trace moisture during the protonation step. We see no evidence of deuterium incorporation at C(7). The intensity of all the hydride peaks relative to the hydrogen on C(2) should be 2:1 if no deuterium is incorporated at the metal core. It is, however, about 1:1. This supports the conclusion that nucleophilic attack is occurring only at the C(7) position of the carbocyclic ring and that protonation is occurring at the metal core. When **2b** is reacted with D^-/H^+ to form **3b**-*dh*, the chemical shifts and peak multiplicities of the aliphatic region change while those in the aromatic region remain consistent with structure **3b**. A decrease in the multiplicity of the resonance centered at 2.64 ppm (m, CH_2(5) and CH_2(7) overlapping) is observed in the ^1H NMR of **3b**-*dh* relative to the peak multiplicities observed for **3b**. The hydride region of the spectrum shows two doublets at −13.72 (d, J_{H-H} = 1.2 Hz) and −13.98 ppm (m, J_{H-H} = 1.2 Hz). The multiplicity of the high-field hydride resonance can be explained by the existence of two isotopomers, where one of the hydride chemical shifts is influenced by being *syn* or *anti* to the C−D bond (Scheme 2). This is consistent with the incorporation of deuterium only at the C(7) position of the carbocyclic ring. There is no evidence of deuterium at either hydride position.

When **2c** is reacted with D^-/H^+ to form **3c**-*dh*, deuterium incorporation occurs at C(7), resulting in two isomers. The deuterium can occupy the C(7) position *cis* or *trans* to the methyl group at C(6). Both isomers are evident in the ^1H NMR of **3c**-*dh* (Scheme 2). The hydride region of the ^1H NMR spectrum of **3c**-*dh* shows two sets of doublets at −13.93 (d, J_{H-H} = 0.8 Hz) and −13.98 (d, J_{H-H} = 0.8 Hz) ppm and at −13.22 (d, J_{H-H} = 0.8 Hz) and −13.86 (d, J_{H-H} = 0.8Hz) ppm , with a relative intensity ratio of 2:1. The aromatic region of the ^1H NMR spectrum of **3c**-*dh* also shows two sets of aromatic resonances in a relative intensity of 2:1. The aliphatic region of **3c**-*dh* shows a multiplet at 2.64 ppm for CH_2(5) and CHD(7) and a multiplet for H(6) at 1.23 ppm. A decrease in the multiplicity is observed at 2.64 ppm for **3c**-*dh* relative to the ^1H NMR spectrum of **3c**. All of these data are consistent with the formation of the proposed *cis* and *trans* isomers (Scheme 2). It would appear that one of the isomers is slightly favored in the case of **3c**-*dh*, but it was not possible to discern which is favored owing to the complexity of the spectrum (the overlap of the multiplets assignable to CH_2(5) and CHD (7)).

There are some interesting contrasts between the ^1H NMR spectra of **3b**-*dh* and **3c**-*dh*. The two sets of hydrides in **3c**-*dh* appear at very different chemical shifts because they belong to two different geometrical isomers, owing to the presence of the methyl group at C(6). In the case of the **3b**-*dh*, the presence of isotopomers (*vide infra*) influences the hydride closest to the C(7)HD group only, probably the hydride on the same edge as the bridging alkylidene. There are two possible isotopomers, which could lead to resolvable differences in the chemical shift. These two isotopomers along with the presence of some **3b** (*vide infra*) cause the upfield hydride in **3b**-*dh* to appear as a multiplet.

We have also examined the reactivity of **1a**−**c** and **2a**−**c** with both H_2 and D_2. Compound **1c** was previously reported to react with H_2 at relatively mild temperatures and pressures (75 °C and 100 psi) to form a mixture of isomeric trihydrides $Os_3(CO)_9(\mu\text{-}\eta^2\text{-(4-Me)-}C_9H_5N)(\mu\text{-H})_3$ and $Os_3(CO)_9(\mu\text{-}\eta^2\text{-(4-Me)}C_9H_5N)H(\mu\text{-H})_2$.[7]

If this reaction is performed at higher temperatures and pressures, dissociation of the ligand from the metal core occurs and no evidence of the reduction of the quinoline ring is observed. If, however, the partially reduced clusters **2a**−**c** are reacted with H_2 at high pressures and moderate temperatures (75 °C and 1000 psi), reduction to **3a**−**c** is observed in high yield (>75%). When **2a** is reacted with D_2 to form **3a**-d_2, incorporation of the deuterium is observed at both the metal core and at the quinoline ligand (eq 5). The aromatic region of the ^{1}H

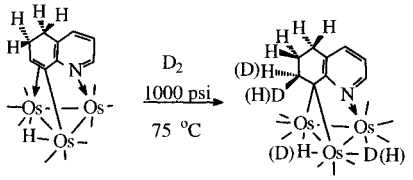

2a **3a-d$_2$** (5)

NMR spectrum of **3a**-d_2 remains identical to that of **3a**. The aliphatic region shows a decrease in the peak multiplicity and intensity for the CH_2(7) multiplet when compared to the ^{1}H NMR spectrum of **3a**. The primary changes occur in the hydride region of the spectrum. A multiplet is observed at −13.73 ppm, and a singlet is observed at −13.95 ppm. The splitting pattern observed in one of the hydride regions of **3a**-d_2 is due to the existence of isotopomers where the chemical shift of the hydride below C(7) is perturbed. The overall integration of both of the hydrides with aromatic resonances is 1:1. Deuterium NMR of **3a**-d_2 shows evidence of deuterium incorporation only in the hydride and aliphatic region at CH_2(7). These results suggest that the reduction of **2a** with D_2 is not reversible, since residual hydrogen is still on the metal core after exposure to a large excess of deuterium.

Without kinetic studies it is difficult to outline a precise mechanism for the apparently irreversible reduction of **2** → **3** with H_2. A likely possibility is reversible rate-determining addition of H_2 to the cluster to form a trihydride intermediate, which then undergoes rapid hydrogen transfer to C(7). Selective transfer of deuterium over hydrogen would be expected based on the lower zero-point energy for the resulting C-D bond . We cannot rigorously exclude a radical chain reaction or a concerted H_2 addition across the cluster ligand interface, but these seem less likely in light of the related chemistry of **1**−**3**.[7]

We previously reported the reaction of tetrahydroquinoline (THQ) with $Os_3(CO)_{10}(CH_3CN)_2$, which results in the formation of two tautomeric products $Os_3(CO)_9(\mu_3\text{-}\eta^2\text{-}C_9H_9N)(\mu\text{-}H)_2$ (**4a**, red; **4b**, yellow (eq 4)). These complexes define a tautomeric equilibrium with an equilibrium constant of 6:1 for **4b**:**4a** at 25 °C. Thermolysis of **4b** in refluxing octane for 24−48 h yields $Os_3(CO)_9(\mu_3\text{-}\eta^2\text{-}C_9H_8N)(\mu\text{-}H)$ (**5**, eq 4).[8] This compound reacts sequentially with $LiBEt_3H$ and CF_3SO_3H to yield the red tautomer **4a** (Scheme 3). When the reaction is conducted with $LiBEt_3D$ followed by protonation with CF_3SO_3H, the isolated red product **4a**-*dh* shows spectral changes only in the aliphatic region of the ^{1}H NMR when compared to the non-deuterated compound **4a.** Compound **4a** shows three aliphatic resonances at 3.49 (m, CH_2(2)), 2.52 (t, CH_2(4)), and 1.57 (m, CH_2(3)) ppm.

Scheme 3

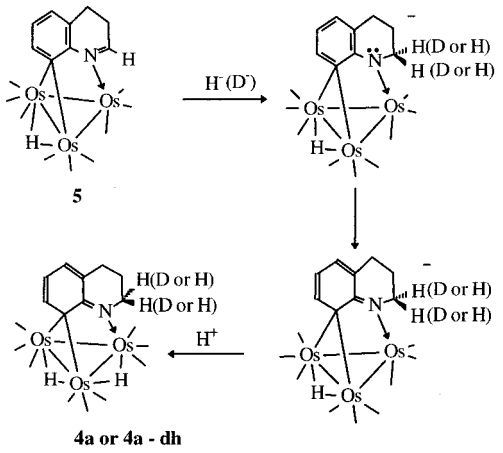

The aliphatic region of the deuterated complex **4a**-*dh* shows evidence of deuterium incorporation at the C(2) position. The multiplicity of both the CH_2(2) and the CH_2(3) is decreased. The relative intensity of the CH_2-(2) resonance decreases to 1:2 relative to the intensity of CH_2(3) and CH_2(4). The hydride region of the ^{1}H NMR of **4a**-*dh* shows two resonances at −13.02 (dd, hydride) and −13.82 (d, hydride) ppm in a 1:1 ratio of relative intensity. The observed splitting pattern indicates that the hydrides are coupled to each other and that one of the hydrides is isotopically shifted by its relation to the deuterium at C(2). Compound **4a**-*dh* has rigid hydrides, and therefore, the hydrogen at C(2) can be in two different locations relative to the hydrides dependent on which face the deuterium nucleophilic attack occurred. Deuterium NMR in CH_2Cl_2 of **4a**-*dh* shows no evidence of deuterium incorporation in the hydride region of the spectrum but does show a strong resonance at 3.67 ppm in CH_2Cl_2. This resonance is very close to the resonance of the hydrogens on C(2) (3.49 ppm) in the ^{1}H NMR spectrum of **4a**. The shift difference is likely due to the change in solvent (CH_2Cl_2 *vs* $CDCl_3$). These ^{1}H and deuterium NMR data are consistent with the mechanism presented in Scheme 3. Nucleophilic attack initially occurs at the C(2) position and is followed by direct protonation at the metal core. Then the lone pair of electrons on the nitrogen form a double bond with C(9), breaking the aromaticity of the carbocyclic ring and allowing the formation of an electron-precise bridging bond at C(8) with two osmium atoms along one edge of the cluster, yielding the complex **4a**-*dh*. Although **5** has the same electron-deficient bonding mode as **2a**−**c**, C(5) is not the site of the nucleophilic attack. In the case of **5**, nucleophilic attack is at C(2), as in free quinolines and as expected for uncoordinated dihydroquinolines where the electronegative nitrogen would make this double bond more electrophilic. Apparently, once the benzenoid character of the heterocyclic ring is disrupted, this electrophilic C=N bond effectively competes with the electron-deficient carbon, C(5), at least for very small nucleophiles like the hydride. This site of attack might be favored further by the expected electron-withdrawing effect of coordination of the nitrogen lone pair to the metal in **5**.

Solid-State Structure of 2a. The solid-state structure of **2a** is shown in Figure 1. The crystal data are

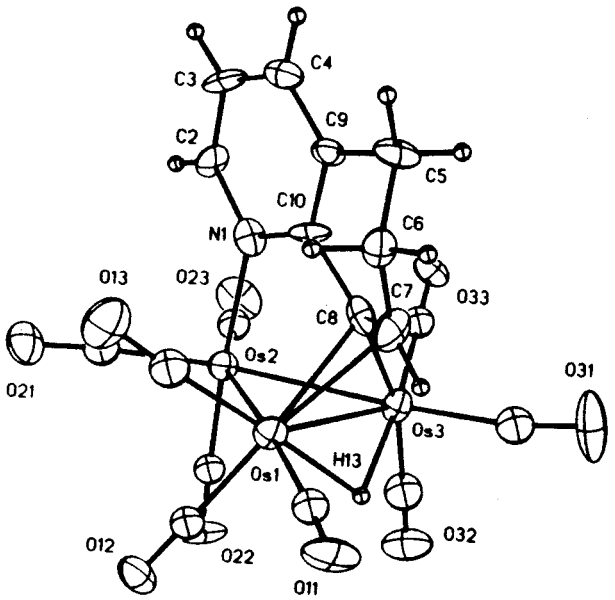

Figure 1. Solid-state structure of $Os_3(CO)_9(\mu_3\text{-}\eta^3\text{-}C_9H_8N)(\mu\text{-}H)$ (**2a**).

given in Table 1. Selected bond distances and angles are given in Table 2. The structure of **2a** consists of an isosceles triangle of Os atoms with the most elongated metal−metal bond being between Os(1) and Os(2) (2.886(1) Å). The hydrides in all the structures reported herein were located using the program HYDEX.[10] The hydride in **2a** is tucked below the plane of the metal triangle. This calculated position for the hydride is confirmed by the position of carbonyl groups CO(13) and CO(33). The most interesting aspects of the structure of **2a** are the carbon−carbon and carbon−nitrogen bond lengths. The N(1)−C(2) (1.35(2) Å) and N(1)−C(10) (1.31(2) Å) bond lengths and those between the carbon atoms (all in the range of 1.33−1.39 Å) indicate that this ring has retained its aromaticity. The C(7)−C(8) bond has been somewhat lengthened (1.38(2) Å) as a result of its σ-π interaction with Os(1) and Os(3) but is still within the range of a carbon−carbon double bond. The C(5)−C(6) bond is clearly a carbon−carbon single bond. The large thermal ellipsoids for C(5) and C(6) suggest some residual motion of these carbons in the solid state, which might be expected given the flexibility of the ring at these saturated centers. The assignment of a σ interaction between Os(3)−C(8) (2.14(2) Å) and a π interaction between Os(1)−C(8) (2.23(2) Å) and Os(1)−C(7) (2.38(2) Å) is consistent with previous studies of σ-π interactions on triosmium clusters.[11]

Solid-State Structure of 3b. The solid-state structure of **3b** is shown in Figure 2, and selected bond distances and bond angles are given in Table 3 and crystal data in Table 1. The structure of **3b** consists of an irregular triangle of osmium atoms with the shortest bond being between Os(2) and Os(3) (2.781(2) Å). This metal−metal bond does not contain a bridging hydride. The longest metal−metal bond is between Os(1)−Os(2) (2.972(1) Å); the hydride bridge on this edge is almost in the plane of the metal triangle, resulting in the elongation of that bond. The Os(1)−Os(3) bond is of intermediate length and has the hydride tucked below the metal plane. It is clear from the C(2)−C(3) (1.37(2) Å) and C(10)−N(1) (1.44(3) Å) bond lengths that the aromaticity of the heterocyclic ring has not been broken up. The other bonds in the heterocyclic ring are <1.37 Å, within the range of carbon−carbon and carbon-nitrogen aromatic bonds. The bond lengths of C(5)−C(6), C(6)−C(7), and C(7)−C(8) are in the range of 1.54−1.56(3) Å and are carbon−carbon single bonds. The thermal ellipsoids of carbons C(5), C(6), and C(7) indicate a large degree of flexibility in the carbocyclic ring. The bonding mode of **3b** at C(8) and N(1) is distinct from that of **1b** due to the reduction of the carbocyclic ring. In **1b**, C(8) forms an equilateral triangle with one edge of the triosmium cluster (Os(1)−C(8), 2.28(2) Å and (Os(2)−C(8), 2.32(2) Å).[7] In compound **3b**, which clearly has two electron-precise σ interactions with Os(1) and Os(3), there is significant distortion in the bonds between C(8) and the cluster (Os(1)−C(8) = 2.21(2) Å and Os(3)−C(8) = 2.04(2) Å). This may be a result of the conformational requirements of the reduced carbocyclic ring or the higher coordination number on Os(1). The Os(2)−N(1) bond length in **3b** (2.13(2) Å) is very similar to the Os(2)−N(1) bonds in **1a** and **2a** (2.13(2) and 2.16(2) Å). This indicates that the Os−N bond length is relatively insensitive to the degree of reduction and to the bonding mode with the cluster of the carbocyclic ring.

Solid-State Structure of 5. The solid-state structure of **5** is shown in Figure 3, selected distances and bond angles are given in Table 4, and crystal data are given in Table 1. The structure of **5** consists of an Os_3 triangle with three slightly different Os−Os bonds (Table 4). The 3,4-dihydroquinoline ligand sits essentially perpendicular to the metal triangle, as is the case for the previously reported **1b**.[7] This structural feature and the almost symmetrical lengths of Os(1)−C(8) and Os(3)−C(8) (2.23(1) and 2.31(1) Å) and their similarity to the same bond lengths in **1b** (2.28(1) and 2.32(1) Å) suggest a three-center two-electron bond between C(8) and Os(1) and Os(3).[7] This is further supported by the bond lengths in the heterocyclic ring (Table 4). Interestingly, both **1b** and **5** show unexpectedly short C(5)−C(6) bond lengths (1.29(1) and 1.33(1) Å, respectively). This may be a reflection of the lower electron density at C(5). The N(1)−C(2) bond is typical for an uncoordinated C−N double bond (1.30(1) Å), while the C(2)−C(3) single bond is significantly shortened (1.44(1) Å). The latter may also reflect the lower electron density at C(2) induced by coordination of the nitrogen lone pair. The Os(2)−N(1) bond length (2.14(1) Å) is very similar to the same bond length in **1b** (2.13(2) Å) and to other related structures.[7]

Solid-State Structure of 6b. We previously assigned a structure to the phosphite adduct of **1b**, $Os_3(CO)_9(\mu\text{-}\eta^2\text{-}C_9H_5(4\text{-Me})N)(\mu\text{-}H)P(OEt)_3$ (**6b**), based on solution ^1H and ^{13}C NMR data.[7] This compound was subjected to both thermolysis and photolysis, and the only products observed were **1b** and nonspecific decomposition. Thus, phosphite substitution apparently blocks formation of the electron-deficient complexes related to **1a**−**c**. This was surprising in light of the fact that **6b** was proposed to be isostructural with the decarbonyl precursors to **1a**−**c**.[7] In order to verify the structure of **6b**, we undertook a solid-state structural investigation.

(10) Orpen, A. G. *J. Chem. Soc., Dalton Trans.* **1980**, 2509.
(11) Clauss, A. D.; Tachikawa, M.; Shapley, J. R.; Pierpont, C. G. *Inorg. Chem.* **1981**, *20*, 1528

Table 1. Crystal Data And Structure Refinement for 2a, 3b, 5, and 6b

identification code	**2a**	**3b**	**5**	**6b**
empirical formula	$C_{18}H_9NO_9Os_3$	$C_{19}H_{13}NO_9Os_3$	$C_{18}H_9NO_9Os_3$	$C_{25}H_{24}NO_{12}Os_3P$
fw	953.86	969.90	953.86	1132.02
temp (K)	228(2)	293(2)	293(2)	293(2)
wavelength (Å)	0.710 73	0.710 73	0.710 73	0.710 73
Cryst syst	monoclinic	monoclinic	monoclinic	triclinic
space group	$P2_1/c$ (No. 14)	$P2_1/n$ (No. 14)	$P2_1/n$ (No. 14)	$P\bar{1}$ (No. 2)
unit cell dimens	$a = 8.986(2)$ Å	$a = 13.805(3)$ Å	$a = 8.803(2)$ Å	$a = 8.643(2)$ Å
	$b = 16.108(5)$ Å	$b = 10.901(2)$ Å	$b = 17.587(4)$ Å	$b = 9.988(2)$ Å
	$c = 14.785(4)$ Å	$c = 15.006(3)$ Å	$c = 13.628(3)$ Å	$c = 18.153(4)$ Å
	$\alpha = 90°$	$\alpha = 90°$	$\alpha = 90°$	$\alpha = 83.65(3)°$
	$\beta = 100.50(2)°$	$\beta = 91.44(3)°$	$\beta = 90.47(3)°$	$\beta = 85.92(3)°$
	$\gamma = 90°$	$\gamma = 90°$	$\gamma = 90°$	$\gamma = 83.22(3)°$
volume (Å^3), Z	2104.2(10), 4	2257.5(11), 4	2109.8(8), 4	1543.9(6), 2
density (calcd) (g/cm^3)	3.011	2.854	3.003	2.435
abs coeff (mm^{-1})	18.120	16.893	18.073	12.426
$F(000)$	1696	1736	1696	1040
cryst size, (mm)	0.20 × 0.15 × 0.13	0.40 × 0.30 × 0.20	0.60 × 0.25 × 0.15	0.5 × 0.2 × 0.13
θ range for data collection (deg)	1.89−25.07	1.98−24.98	1.89−27.99	1.13−27.97
limiting indices	$-10 \le h \le 10$, $0 \le k \le 18$, $-17 \le l \le 17$	$0 \le h \le 16$, $-12 \le k \le 12$, $-17 \le l \le 17$	$-11 \le h \le 11$, $0 \le k \le 23$, $-17 \le l \le 17$	$-11 \le h \le 11$, $-12 \le k \le 13$, $-23 \le l \le 23$
no. of reflns colld	7888	8271	10 504	14 864
no. of indep reflns	3691 ($R_{int} = 0.088$)	3958 ($R_{int} = 0.0654$)	5090 ($R_{int} = 0.058$)	7434 ($R_{int} = 0.043$)
abs corr	ψ	ψ	ψ	ψ
max and min transmission	0.9999, 0.7982	0.9980, 0.6709	0.9992, 0.6335	0.998, 0.583
refinement method	full-matrix least-squares on F^2	full-matrix least-squares on F^2	full-matrix least-squares on F^2	full-matrix least-squares on F^2
data/restraints/params	3690/0/236	3953/0/190	5088/0/235	7434/0/380
goodness-of-fit on F^2	0.801	2.272	0.848	0.993
final R indices [$I > 2\sigma(I)$]	R1 = 0.0462, wR2 = 0.0632	R1 = 0.0736, wR2 = 0.1310	R1 = 0.0388, wR2 = 0.0622	R1 = 0.0361, wR2 = 0.0584
R indices (all data)	R1 = 0.1066, wR2 = 0.0862	R1 = 0.0841, wR2 = 0.1507	R1 = 0.0672, wR2 = 0.1080	R1 = 0.0560, wR2 = 0.0752
ext coeff	$2.8(2) \times 10^{-4}$	$2.02(11) \times 10^{-3}$		$1.04(4) \times 10^{-3}$
largest diff. peak and hole (e Å^3)	1.096, −1.035	4.130, −4.888	1.029, −0.847	1.317, −1.319

Table 2. Selected Bond Lengths (Å) and Bond Angles (deg) for 2a[a]

Bond Lengths			
Os(1)−Os(2)	2.886(1)	C(5)−C(9)	1.53(2)
Os(1)−Os(3)	2.837(1)	C(4)−C(9)	1.39(2)
Os(2)−Os(3)	2.771(1)	C(3)−C(4)	1.32(3)
Os(1)−C(7)	2.38(2)	C(2)−C(3)	1.34(2)
Os(1)−C(8)	2.23(2)	C(2)−N(1)	1.35(2)
Os(2)−N(1)	2.16(2)	C(10)−N(1)	1.31(2)
Os(3)−C(8)	2.14(2)	C(9)−C(10)	1.38(2)
C(7)−C(8)	1.38(2)	C(1)−C(2)	1.47(2)
C(6)−C(7)	1.54(2)	Os−CO[b]	1.87
C(6)−C(5)	1.54(2)	C−O[b]	1.14

Bond Angles			
Os(1)−Os(2)−Os(3)	60.20(3)	Os(1)−Os(3)−C(8)	50.8(5)
Os(1)−Os(3)−Os(2)	61.9(3)	Os(3)−Os(1)−C(8)	48.0(4)
Os(2)−Os(1)−Os(3)	57.89(3)	C(7)−Os(1)−Os(2)	104.9(5)
Os(1)−Os(2)−N(1)	85.8(4)	C(7)−Os(1)−Os(3)	71.1(5)
Os(2)−Os(3)−N(1)	87.0(4)	Os−C−O[b]	176.3

[a] Numbers in parentheses are estimated standard deviations. [b] Average values.

Table 3. Selected Bond Lengths (Å) and Bond Angles (deg) for 3b[a]

Bond Lengths			
Os(1)−Os(2)	2.972(1)	C(9)−C(5)	1.46(2)
Os(1)−Os(3)	2.810(2)	C(5)−C(6)	1.54(3)
Os(2)−Os(3)	2.781(2)	C(6)−C(7)	1.56(3)
Os(1)−C(8)	2.21(2)	C(7)−C(8)	1.55(3)
Os(3)−C(8)	2.04(2)	C(8)−C(10)	1.63(3)
Os(2)−N(1)	2.13(2)	C(9)−C(10)	1.36(3)
C(2)−C(3)	1.37(2)	C(10)−N(1)	1.44(3)
C(3)−C(4)	1.43(3)	C(2)−N(1)	1.31(2)
C(4)−C(9)	1.36(3)	Os−CO[b]	1.94
C(4)−C(1)	1.50(3)	C−O[b]	1.10

Bond Angles			
Os(3)−Os(1)−Os(2)	57.41(3)	N(1)−Os(2)−Os(3)	84.6(4)
Os(2)−Os(3)−Os(1)	64.22(4)	C(7)−C(8)−C(10)	106(2)
Os(3)−Os(2)−Os(1)	58.37(4)	C(7)−C(8)−Os(3)	119(2)
C(8)−Os(3)−Os(2)	79.2(6)	C(7)−C(8)−Os(1)	114(1)
C(8)−Os(1)−Os(3)	46.1(5)	Os−C−O[b]	174.7

[a] Numbers in parentheses are estimated standard deviations. [b] Average values.

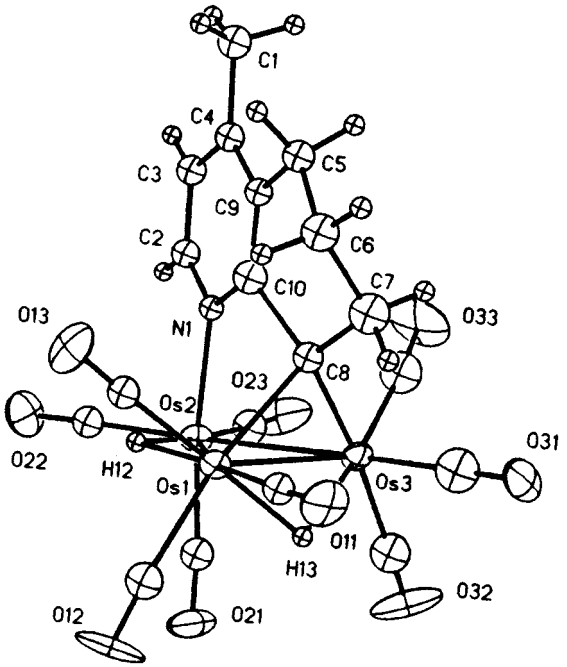

Figure 2. Solid-state structure of $Os_3(CO)_9(\mu_3\text{-}\eta^2\text{-}(4\text{-Me})C_9H_8N)(\mu\text{-}H)_2$ (**3b**).

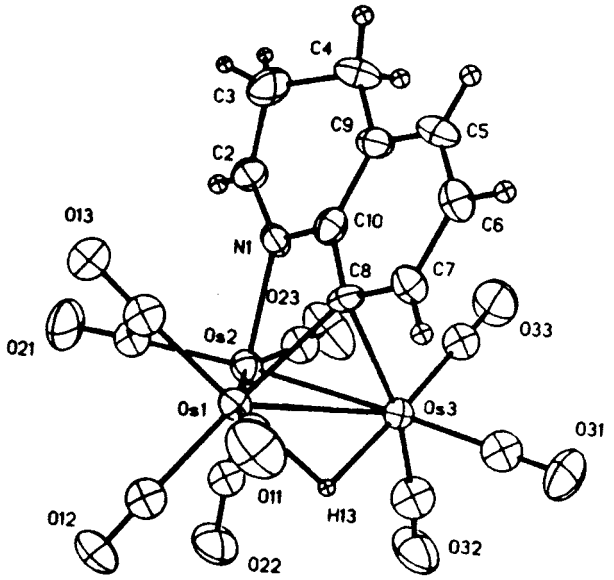

Figure 3. Solid-state structure of $Os_3(CO)_9(\mu_3\text{-}\eta^2\text{-}C_9H_8N)(\mu\text{-}H)$ (**5**).

The solid state structure of **6b** is shown in Figure 4, and selected bond lengths and bond angles are given in Table 5 and crystal data in Table 1. The solid-state structure of **6b** consists of an isosceles triangle of osmium atoms with the elongated edge bridged by an in-plane hydride and the 4-methylquinoline ligand. The bond lengths of the carbocyclic ring fall in the range of 1.33(1)−1.44(1) Å, suggesting unperturbed benzenoid character in the ring. The heterocyclic ring also has bond lengths consistent with benzenoid character, bond lengths ranging from 1.38(1) to 1.44(1) Å. The longest bond in both rings is the C(9)−C(10) bond (1.44(1) Å). The location of the $P(OEt)_3$ ligand under the C(8) carbon can only result from both carbonyl and ligand migration on reaction of phosphite with **1b**. The structure of **6b** does not shed light on the reasons for why **6b** does not rearrange to an analog of **1** upon thermolysis or photolysis.

Selective CO Incorporation into 1. The regioselective formation of **6b** from **1b** prompted us to investigate whether the reaction with CO is also regioselective. When a sample of **1b** is exposed to 1 atm of ^{13}CO and the ^{13}C NMR monitored within 30 min, selective enrichment into one position at 177.23 ppm is observed. Seven additional resonances at 183.57, 182.58, 177.41, 176.81, 176.60, 175.75, and 175.40 ppm are observed, all in a relative integrated intensity of 35−40% of the resonance at 177.23 ppm. In addition, two resonances at 177.14 and 175.28 ppm appear in a relative intensity of <10% of the resonance at 177.23 ppm (Figure 5a). After the sample was allowed to stand at ambient temperatures for ~2 days, all 10 resonances appear at approximately equal relative intensities (Figure 5b). This spectrum is identical with that of a natural-abundance sample of $Os_3(CO)_{10}(\mu\text{-}\eta^2\text{-}(4\text{-Me})C_9H_5N)(\mu\text{-}H)$ (**7b**). Partial assignment of all 10 resonances can be made from analysis of the proton-coupled spectrum, the 2D-^{13}C EXSY spectrum (Figure 6), and from trends in the ^{13}C NMR data in related triosmium clusters.[12] The resonances at 183.57, 182.58, 177.41, and 174.75

(12) Day, M.; Espitia, D.; Hardcastle, K. I.; Kabir, S. E.; McPhillips, T.; Rosenberg, E. *Organometallics* **1993**, *12*, 2309.

Table 4. Selected Bond Lengths (Å) and Bond Angles (deg) for 5[a]

Bond Lengths			
Os(1)−Os(2)	2.759(1)	N−C(2)	1.30(1)
Os(1)−Os(3)	2.772(1)	C(2)−C(3)	1.44(1)
Os(2)−Os(3)	2.776(1)	C(3)−C(4)	1.50(1)
Os(1)−C(8)	2.23(1)	C(4)−C(9)	1.51(1)
Os(3)−C(8)	2.31(1)	C(5)−C(9)	1.39(1)
Os(2)−N	2.14(1)	C(5)−C(6)	1.33(1)
Os−CO[b]	1.90(1)	C(6)−C(7)	1.36(1)
C−O[b]	1.12(1)	C(7)−C(8)	1.39(1)
		C(8)−C(9)	1.40(1)

Bond Angles			
Os(1)−Os(2)−Os(3)	60.11(2)	N−C(2)−C(3)	124.(1)
Os(1)−Os(3)−Os(2)	59.6(2)	C(2)−N−C(10)	118.(1)
Os(2)−Os(1)−Os(3)	60.27(2)	C(10)−C(9)−C(5)	116.(1)
Os(2)−N−C(1)	123.(1)	C(10)−C(9)−C(4)	120.(1)
Os(2)−N−C(10)	118.(1)	C(10)−C(9)−N	118.(1)
Os(3)−Os(1)−C(8)	53.7(3)	Os−C−O[b]	177.(1)
Os(2)−Os(3)−C(8)	78.2(2)		

[a] Numbers in parentheses are estimated standard deviations. [b] Average values.

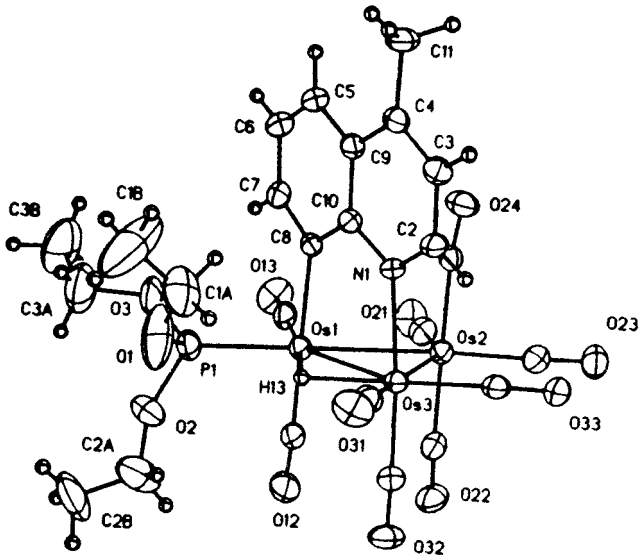

Figure 4. Solid-state structure of $Os_3(CO)_9(\mu_3\text{-}\eta^2\text{-}(4\text{-Me})C_9H_5N)(\mu\text{-H})$ $P(OEt)_3$ (**6b**).

Table 5. Selected Bond Lengths (Å) and Bond Angles for 6b[a]

Bond Lengths			
Os(1)−Os(2)	2.931(1)	C(5)−C(6)	1.33(1)
Os(2)−Os(3)	2.889(1)	C(5)−C(9)	1.40(1)
Os(1)−Os(3)	2.866(1)	C(4)−C(9)	1.40(1)
Os(1)−C(8)	2.17(1)	C(3)−C(4)	1.38(1)
Os(3)−N(1)	2.17(1)	C(2)−C(3)	1.39(1)
Os(1)−P(1)	2.26(1)	C(9)−C(10)	1.44(1)
N(1)−C(10)	1.41(1)	C(4)−C(11)	1.50(1)
N(1)−C(2)	1.32(1)	P(1)−O(1)	1.57(1)
C(8)−C(10)	1.41(1)	P(1)−O(2)	1.58(1)
C(7)−C(8)	1.36(1)	P(1)−O(3)	1.55(1)
C(6)−C(7)	1.41(1)		

Bond Angles			
Os(3)−Os(1)−Os(2)	59.77(2)	C(8)−Os(1)−Os(2)	89.7(2)
Os(3)−Os(2)−Os(1)	58.99(3)	C(8)−Os(1)−Os(3)	83.9(2)
Os(1)−Os(3)−Os(2)	61.24(2)	C(8)−Os(1)−P	89.4(2)
N(1)−Os(3)−Os(1)	84.9(2)	P−Os(1)−Os(2)	176.77(8)
N(1)−Os(3)−Os(1)	91.4(2)	Os−CO[b]	176.11

[a] Numbers in parentheses are estimated standard deviations. [b] Average values.

ppm can be assigned to the $Os(CO)_4$ group in **7b** from the 2D ^{13}C EXSY cross peaks, which indicate the presence of a sequential two-stage tripodal motion as previously observed in related decacarbonyl triosmium clusters.[12] These resonances show no hydrogen coupling and are slightly broadened at ambient temperatures. No cross peaks are observed for the other six resonances. These resonances can be assigned from the relative magnitude of their hydrogen couplings.[10] Thus, the resonance at 176.60 ppm can be assigned to the CO *trans* to the hydride on the osmium atom bound to nitrogen ($^2J(^{13}C^1H)$ = 12.1 Hz). This assignment is based on an analogy with a large number of triosmium complexes having an edge doubly bridged by a hydride and nitrogen heterocycle. In several cases where the bridging hydride has been located, the bridge is asymmetric with the metal−hydride bond being much shorter to the nitrogen-bound metal and exhibiting larger $^2J(^{13}C^1H)$ to the carbonyls.[13] The carbonyl *trans* to the hydride on the osmium atom bound to carbon can be assigned to the resonance at 175.75 ($^2J(^{13}C^1H)$ = 9.1 Hz). The radial carbonyls *cis* to the hydride on the carbon- and nitrogen-bound osmium atoms can be assigned to the resonances at 177.23 ($^2J(^{13}C^1H)$ = 3.8 Hz) and 176.81 ppm ($^2J(^{13}C^1H)$ = 4.5 Hz), respectively, while the axial carbonyls on these respective osmium atoms can be assigned to the resonances at 177.14 ($^2J(^{13}C^1H)$ < 1 Hz) and 175.28 ppm ($^2J(^{13}C^1H)$ = 3.0 Hz). These latter assignments utilize the trend $^2J(^{13}C^1H)$ radial-*trans* > radial-*cis* > axial.[12] The complete as-

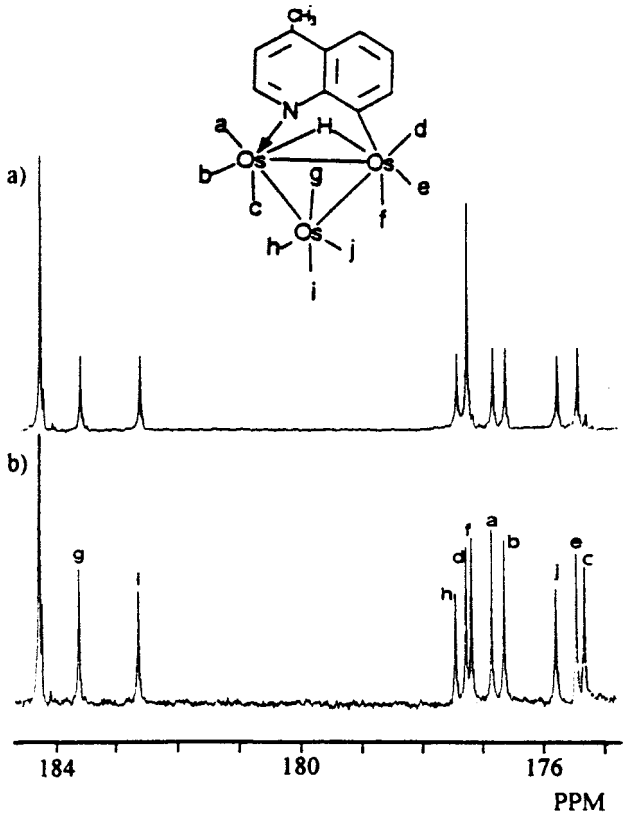

Figure 5. Proton-decoupled ^{13}C NMR at 100 MHz in $CDCl_3$ of $Os_3(CO)_9(\mu_3\text{-}\eta^2\text{-}(4\text{-Me})C_9H_5N)(\mu\text{-H})$ (**1b**) in the carbonyl region after exposure to 1 atm of 90% ^{13}CO: (a) within 30 min after exposure; (b) 2 days after exposure (large peak is free CO).

(13) Gobetto, R.; Hardcastle, K. I.; Kabir, S. E.; Milone, L.; Nishimura, N.; Botta, M.; Rosenberg, E.; Yin, M. *Organometallics* **1995**, *14*, 3068 and references therein.

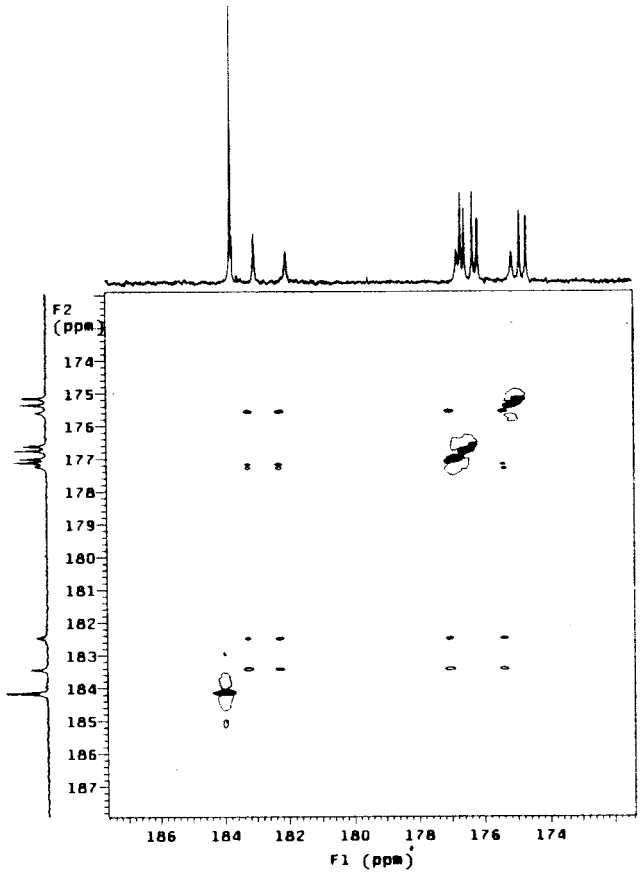

Figure 6. ^{13}C-EXSY spectrum of $Os_3(CO)_9(\mu_3\text{-}\eta^2\text{-}(4\text{-Me})C_9H_5N)(\mu\text{-H})$ (**1b**) after exposure to ^{13}CO for 2 days in the carbonyl region at 100 MHz in $CDCl_3$ at 50 °C (large peak is free CO).

signment is illustrated in Figure 5. Given these assignments, the radial carbonyl group *cis* to the hydride on the osmium bound to C(8) of the quinoline ring is the most enriched while the axial carbonyls on the doubly bridged edge of the cluster are the least enriched.

If one considers initial attack at the electron-deficient doubly bridged edge of **1b,** four isotopomers of **7b** would be obtained (structures **A, B, C,** and **D**; Scheme 4). The expected initial relative populations of these isotopomers would be **A** > **B** ≈ **C** > **D** based on the two-stage tripodal motion demonstrated for this type of $Os(CO)_4$ group.[12] From these initially formed isotopomers, three processes could occur which result in the formation of **7b**: (1) hydride migration; (2) carbon and hydrogen migration; (3) nitrogen migration. Simple hydrogen migration would leave all of the labels on the $Os(CO)_4$ group. Carbon and hydrogen migration from the most populated isotopomer coupled with a "merry-go-round" intramolecular carbonyl migration in a plane perpendicular to the metal triangle would move the label into a radial position *cis* to the hydride.[14] This rearrangement is likely to be the fastest, but nitrogen migration must also be accessible since significant ^{13}CO incorporation is also seen at the nitrogen-bound osmium atom. Similar rearrangements from isotopomer **B** would leave the label unchanged (nitrogen migration) or move it to the axial position (carbon migration) and *vice-versa* for isotopomer **C**. Note that for isotopomer

Scheme 4

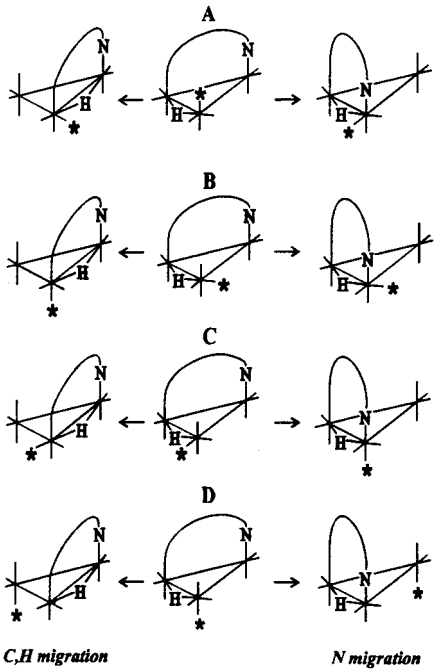

D, both carbon and nitrogen migration would move the label off the doubly bridged edge of **7b**. This fact along with the initial lower population of **D** would account for the lower ^{13}CO incorporation in the axial positions on the doubly bridged edge. In order to rationalize the fact that seven of the carbonyl resonances are of equal intensity, we should probably include an in-plane merry-go-round process in the overall dynamical process. However, this process must be slower or no selective enrichment of carbonyl d (Figure 5) would be observed. We have recently demonstrated very similar rearrangements in the μ_3 to μ interconversion of trimetallic imidoyl complexes.[15] Randomization of the label could occur by slower axial−radial scrambling at the doubly bridged edge or by intermolecular processes or both. The greater facility of carbon migration apparently observed here is consistent with its ability to form a three-center two-electron bond as in **1**. It may be that the inability of **6b** to form analogs of **1** arises from the impact the phosphine has on the migratory aptitude of the C(8) carbon of the quinoline ring.

Electrochemical Studies of 1. Compounds **1a**−**c** are closely related to the green 46-electron cluster $Os_3(CO)_8(\mu_3\text{-}\eta^3\text{-}(C_6H_5)_2PCH_2P(C_6H_5)C_6H_4)(\mu\text{-H})$ in that both possess a bridging phenyl bound to the cluster by a three-center two-electron bond.[16] The electrochemistry of this diphosphine derivative has been studied in detail and exhibits a 1-electron chemically reversible reduction at −1.18 V. ESR studies revealed that this reduction was metal based. In view of the fact that hydrides and carbanions attack **1a**−**c** at the 5-position of the quinoline ring while phosphines, amines, and H_2 react at the metal core, we thought it would be instructive to examine the electrochemical behavior of **1a**.[7,9]

The polarographic response of **1a** was investigated in dichloromethane solution, containing $[NBu_4][PF_6]$ as the

(14) Alex, R. F.; Pomeroy, R. K. *Organometallics* **1987**, *6*, 2437.

(15) Rosenberg, E.; Hajela, S.; Day, M.; Hardcastle, K. I.; Moizeau, K.; Wolf, E.; Milone, L.; Osella, D.; Gobetto, R. *Organometallics* **1997**, *16*, 2665.

(16) Osella, D.; Ravera, M.; Smith, A. K.; Mathews, A. J.; Zanello, P. *J. Organomet. Chem.* **1992**, *423*, 255.

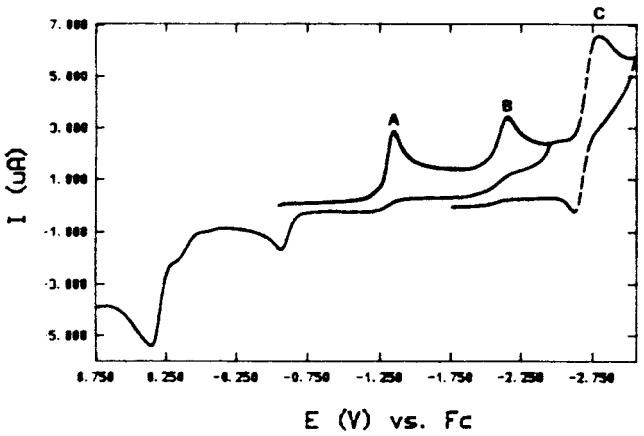

Figure 7. Cyclic voltamogram of $Os_3(CO)_9(\mu_3\text{-}\eta^2\text{-}C_9H_6N)(\mu\text{-}H)$ (**1a**) in CH_3CN at 200 m Vs^{-1}.

supporting electrolyte and ferrocene (Fc) as an internal standard. Two one-electron metal-centered reduction waves (A and B, respectively) are observed at $E_{1/2}(A) = -1.38$ V and $E_{1/2}(B) = -1.99$ V (*vs* Fc), confirming the overall electronic unsaturation of the 46-electron cluster **1a**. Polarographic logarithmic analysis indicates the Nernstian behavior of the first reduction process (60 mV slope of the log plot), while the second process appears to be slightly irreversible. The one-electron consumption associated with wave A was further checked by controlled-potential coulometry at a mercury pool ($E_{appl} = 1.4$ V *vs* Fc). The total disappearance of the second wave B after one-electron electrolysis indicates that the first reduction produces a very unstable 47-electron intermediate. The kinetics of the chemical reaction coupled with the first one-electron reduction (wave A) was evaluated by using ac polarography: the analysis of the data provided a rate constant of the homogeneous chemical reaction $k_1 = 910$ s^{-1} and a reversible half-wave potential $E_{1/2}(A) - 1.35$ V (*vs* Fc). Similar treatment for the second wave B showed ever higher instability of the 47-electron species: $k_2 = 3000$ s^{-1}.

More informative is the cyclic voltammetric (CV) response of **1a** in acetonitrile solution. (Figure 7). Two one-electron reduction peaks are observed at $E_p(A) = -1.36$ V and $E_p(B) = -2.02$ V (*vs* Fc), respectively (scan rate = 200 mV s^{-1}). These two metal-centered reductions show no associated reoxidation peaks at scan rates as high as 50 V and temperatures as low as −20 °C, confirming the fast chemical complications following both reductions. Reoxidation peaks of decomposition products appear at anodic potentials. A third reduction process (C), almost chemically reversible, appears at $E_p = -2.65$ V (*vs* Fc), a behavior very similar to that exhibited by free quinoline (tested in identical experimental conditions). This supports a detachment of the aromatic ring after two-electron reduction at the metal core. This overall behavior is not very similar to that observed for the diphosphine derivatives referred to above.[16]

The diphosphine derivatives are easier to reduce overall and show reversible behavior for the first one-electron reduction. It would appear that **1a** is subject to very rapid decomposition, even after the first one-electron reduction, since trying to reoxidize it after the first one-electron reduction failed to give reversible behavior. This could be ascribed to the greater stability of the metal−phosphorous interactions relative to the metal−carbon and metal−nitrogen bonds in **1a**. On the other hand, two one-electron electron reductions are found for **1a** at <-2.00 V, as expected for a 46-electron species, while the diphosphine derivatives show only a single one-electron reduction in this range. It would be interesting to see if the bridging phenyl groups in $Os_3(CO)_8(\mu_3\text{-}\eta^3\text{-}Ph_2PCH_2PPhC_6H_4)(\mu\text{-}H)$ exhibit the same reactivity toward nucleophiles as that observed for **1**.

Ligand Dynamics of 2. The complexes **2a**−**c** belong to the class of cluster derivatives known as $\mu\text{-}\eta^2\text{-}\sigma\text{-}\pi$-vinyl compounds. A characteristic feature of this bonding mode is the facile σ-π-interchange.[11,17] Compounds **2a**−**c** have the additional feature of having the vinyl group as part of a relatively rigid ring system tethered to the third metal atom via a very rigid fused second ring. We were curious as to whether these additional structural constraints would influence the barrier to the σ-π-interchange, and so we undertook a variable-temperature (VT) ^{13}C NMR study of **2b** to investigate this point. The variable-temperature ^{13}C NMR of **2b** is shown in Figure 8. At −80 °C, nine resonances of equal relative integrated intensities are observed, as expected for the static C_1 symmetry of **2b**, at 186.32, 185.17, 183.43, 182.60, 179.96, 178.89, 177.87, 177.35, and 171.4 ppm. As the temperature is increased, these resonances broaden and coalesce to five resonances at +22 °C at 186.09, 182.60, 180.48, 178.96, and 175.36 ppm (relative integrated intensity = 2:1:2:2:2), as be expected from the plane of symmetry introduced by the σ-π-vinyl interchange. This motion should interchange pairs of carbonyls only. Although this is not obvious from the VT-^{13}C NMR due to fortuitous overlap of resonances in the intermediate exchange regime, it is very clear from the 2D-^{13}C EXSY spectrum at −80 °C (Figure 9). A lineshape analysis of the averaging of the two most downfield resonances which are involved in the pairwise exchange gave an activation energy of 39.7 ± 2 kJ/mol. Using a coalescence temperature of −65 °C, an activation free energy of 41.0 ± 2 kJ/mol is obtained. These values are slightly lower than those reported for acyclic σ-π-vinyls (43.0−47.2 kJ/mol).[11] This slightly lower value could arise from the ring puckering observed in **2b** (Figure 1), which would raise the energy of the ground state relative to the acyclic σ-π-vinyl complexes previously reported.

Experimental Section

All reactions were performed under a dry nitrogen atmosphere. Dichloromethane was distilled from CaH_2 prior to use. Quinoline (Aldrich) and 1,2,3,4-tetrahydroquinoline (Aldrich) were vacuum distilled from CaH_2. Trifluoromethanesulfonic acid and lithium triethylborohydride were purchased from Aldrich. Osmium carbonyl was purchased from Strem Chemicals. Compounds **1a**−**c**, **2a**−**c**, **3a**−**c**, **4a**, **4b**, **5**, and **6b** were prepared according to published procedures.[7,8] Thin-layer chromatography was performed on 20 × 40 cm glass plates using a 2 mm layer of silica gel PF-254 (E & M Science). Two or three elutions were necessary to obtain adequate resolution of the bands. NMR solvents were stored over molecular sieves (Mallincrodt 4A). Reactions involving deuterated compounds were done in a M-Braun manual MB-150-M drybox. Hydrogenations were done in a Parr 50 mL kinetic hydrogenator.

(17) Aime, S.; Gobetto, R.; Osella, D.; Milone, L.; Rosenberg, E.; Anslyn, E. V. *Inorg. Chim. Acta* **1986**, *111*, 95.

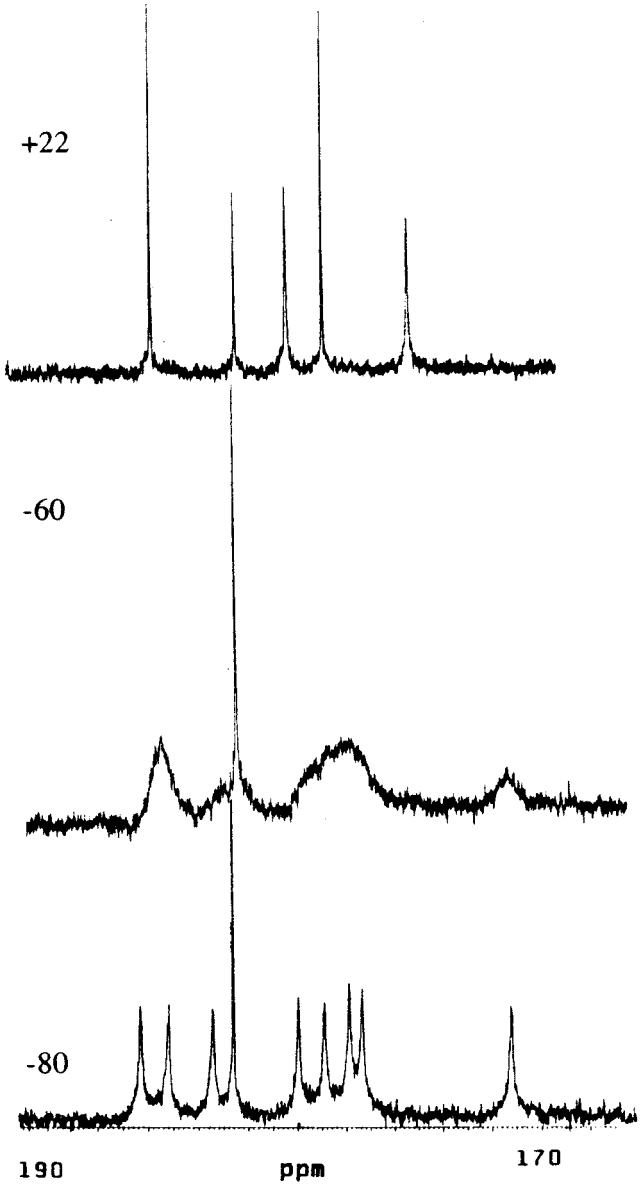

Figure 8. VT ^{13}C NMR of $Os_3(CO)_9(\mu_3\text{-}\eta^3\text{-}(4\text{-Me})C_9H_7N)(\mu\text{-}H)$ (**2b**) in the carbonyl region at 100 MHz in CD_2Cl_2.

Infrared spectra were recorded on a PE-1420 spectrophotometer. NMR spectroscopy was done on a Varian 400 MHz Unity Plus NMR or a Jeol EX400 NMR.

Electrochemical Measurements. Voltammetric and polarographic measurements were performed with a PAR 273 electrochemical analyzer connected to an interfaced PC. A three-electrode cell was designed to allow the tip of the reference electrode (SCE) to closely approach the working electrode. Compensation for the *iR* drop was applied through positive-feedback device. All measurements were carried out under nitrogen in anhydrous deoxygenated solvents. Solutions were 1×10^{-3} M for the compounds under study and 1×10^{-1} M for the supporting electrolyte, $[Bu_4N][BF_4]$. The temperature of the solution was kept constant (±1 °C), by circulation of a thermostated water/ethanol mixture through a jacketed cell. The working electrode was a hanging mercury drop electrode (HMDE) or dropping mercury electrode (DME). Potential data (*vs* SCE) were referred to the ferrocene (0/1+) couple; under the actual experimental conditions, the ferrocene/ferrocenium couple is located at +0.46 V in methylene chloride and at +0.40 V *vs* SCE in acetonitrile.

Reaction of $Os_3(CO)_9(\mu_3\text{-}\eta^2\text{-}(6\text{-Me})C_9H_5N)(\mu\text{-}H)$ (1c) with $LiEt_3BX$ and CF_3SO_3X (X = H or D). Dark green crystals of **1c** (150 mg, 0.155 mmol) were dissolved in 30 mL of CH_2Cl_2 in a drybox. A 1.0 M solution of $LiEt_3BH$ (175 μL, 0.175 mmol) in 20 mL of CH_2Cl_2 was then added dropwise to the cluster solution, and a color change was observed from dark green to light yellow. The solution was then neutralized with CF_3SO_3H (18 μL, 0.18 mmol). A color change was observed from light yellow to orange. The solution was removed from the drybox, and the solvent was removed *in vacuo*. The residue was then chromatographed by TLC on silica gel. Elution with hexane/CH_2Cl_2 (3:1) gave two resolved bands. The faster moving band afforded **3c** (15 mg, 10% yield), while the slower moving band offorded **2c** (113 mg, 75%). The preparation of **2c**-d_2 was performed by the above method in a 73% yield. The preparation of **2c**-*dh* was also performed by the above method in a 70% yield. **2a,b** were also prepared by the above method in 72% and 75% yields, respectively, and their analytical data were previously published.[7]

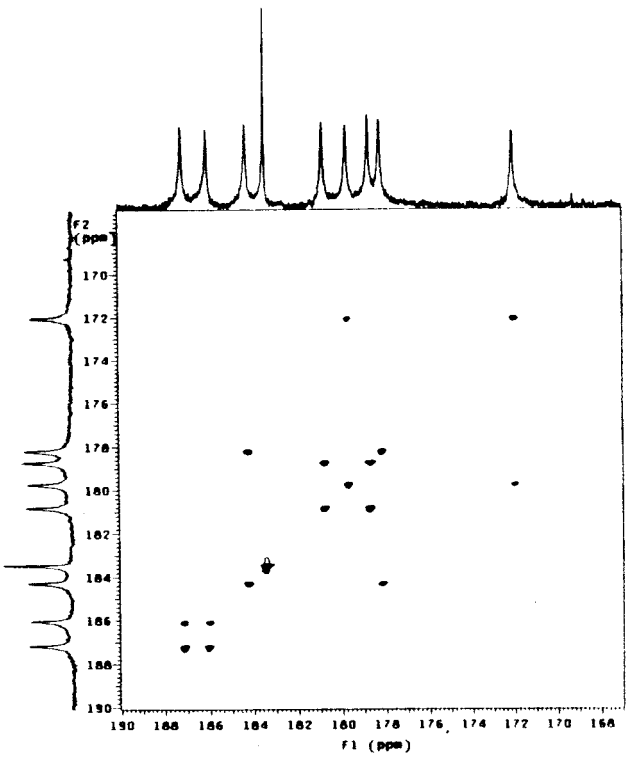

Figure 9. ^{13}C-EXSY spectrum of $Os_3(CO)_9(\mu_3\text{-}\eta^3\text{-}(4\text{-Me})C_9H_7N)(\mu\text{-}H)$(**2b**) in the carbonyl region at −80 °C at 100 MHz in CD_2Cl_2.

Spectroscopic Data for 2c, 2c-d_2, and 2c-*dh*. ^1H NMR of **2c** (400 MHz, $CDCl_3$): δ 8.40 (dd, H(2)), 6.77 (dd, H(3)), 7.35 (dd, H(4)), 2.17 (m, H(6)), 3.71 (d, H(7)), 1.27 (d, CH_3), 2.45 (m, CH_2(5)), −17.00 (s, hydride). ^1H NMR of **2c**-d_2 (400 MHz, $CDCl_3$): δ 8.40 (dd, H(2)), 6.77 (dd, H(3)), 3.71 (s, H(7)), 7.36 (dd, H(4)), 3.70 (s, H(7)), 1.27 (s, CH_3), 2.41 (s, CDH(5)), 2.54 (s, CHD(5)), −17.01 (s, hydride). ^1H NMR of **2c**-*dh* (both isomers, 400 MHz, $CDCl_3$): δ 8.40 (dd, H(2)), 6.77 (dd, H(3)), 7.35 (dd, H(4)), 2.17 (m, H(6)), 3.71 (d, H(7)), 1.27 (s, CH_3), 2.41 (d, H(5), *cis* J_{H-H} = 4.4 Hz), 2.52 (d, H(5), *trans* J_{H-H} = 11.2 Hz), −17.00 (s, hydride).

Reaction of 2b or 2c with $LiEt_3BX$ and CF_3SO_3X (X = H or D). Orange crystals of **2b** (75 mg, 0 .077 mmol) were dissolved in 20 mL of CH_2Cl_2 in a drybox. A 1.0 M solution of $LiEt_3BH$ (100 μL, 0.1 mmol) in 15 mL of CH_2Cl_2 was then added dropwise to the cluster solution, and a color change was observed from orange to light yellow. The solution was then neutralized with CF_3SO_3H (11 μL, 0.11 mmol). The solution was then removed from the drybox, and the solvent was removed under vacuum. The residue was chromatographed by TLC on silica gel. Elution with hexane/CH_2Cl_2 (3:1) gave

two bands. The faster moving band afforded **3b** (53 mg, 70% yield), and the slower moving band afforded unreacted **2b**. Compounds **3b**-*hd*, **3b**-*dh*, and **3c**-*dh* were also prepared according to the above method in similar yield.

Spectroscopic Data for Compound 3b. ^{1}H NMR of **3b** (400 MHz, $CDCl_3$): δ 8.05 (d, H(2)), 6.28 (d, H(3)), 2.03 (s, CH_3), 2.64 (m, CH_2(5), CH_2(7)), 1.68 (m, CH_2(6)), −13.86 (d, J_{H-H} = 1.2 Hz, hydride), −13.99 (d, J_{H-H} = 1.2 Hz, hydride). ^{1}H NMR of **3b**-*hd* (400 MHz, $CDCl_3$): δ 8.05 (d, H(2)), 6.28 (d, H(3)), 2.03 (s, CH_3), 2.63 (m, CH_2(5), CH_2(7)), 1.68 (m, CH_2(6)), −13.85(s, hydride), −13.98(s, hydride) . ^{1}H NMR of **3b**-*dh* (400 MHz, $CDCl_3$): δ 8.09 (d, H(2)), 6.35 (d, H(3)), 1.98 (s, CH_3), 2.63 (m, CH_2(5), CHD(7)), 1.81 (m, CH_2(6)), −13.72 (d, J_{H-H} = 1.2 Hz, hydride), −13.98 (m, J_{H-H} = 1.2 Hz, hydride). ^{1}H NMR of **3c**-*dh* (minor isomer; 400 MHz, $CDCl_3$): δ 8.15 (d, H(2)), 6.37 (dd, H(3)), 7.23 (d, H(4)), 2.64 (m, CH_2(5), CDH(7)), 1.23 (m, H(6)), 1.53 (d, CH_3) −13.22 (d,J_{H-H} = 0.8 Hz, hydride), −13.86 (d, J_{H-H} = 0.8 Hz hydride). ^{1}H NMR of **3c**-*dh* major isomer; 400 MHz, $CDCl_3$): δ 8.17 (d, H(2)), 6.42 (dd, H(3)), 7.23 (d, H(4)), 2.64 (m, CH_2(5), CDH(7)), 1.24 (m, H(6)), 1.53 (d, CH_3), −13.93 (d, J_{H-H} = 0.8 Hz, hydride), −13.98 (d, J_{H-H} = 0.8 Hz, hydride).

Reaction of $Os_3(CO)_9(\mu_3$-η^2-$C_9H_8N)(\mu$-H) (5) with $LiEt_3BD$ and CF_3SO_3H. Dark green crystals of **5** (110 mg, 0.111 mmol) were dissolved in 25 mL of CH_2Cl_2 in a drybox. A 1.0 M solution of $LiEt_3BD$ (130 μL, 0.13 mmol) in 20 mL of CH_2Cl_2 was then added dropwise to the cluster solution, and a color change was observed from dark green to light yellow. The solution was then neutralized with CF_3SO_3H (12 μL, 0.12 mmol). A color change was observed from light yellow to dark red. The solution was removed from the drybox, and the solvent was removed on a rotary evaporator. The residue was then chromatographed by TLC on silica gel. Elution with hexane/CH_2Cl_2 (3:1) gave one resolved band of $Os_3(CO)_9(\mu_3$-η^2-C_9H_8(D)N)(μ-H) (**4a**-*dh*) (81 mg, 0.085 mmol, 74% yield).

Spectroscopic Data for Compound 4a-*dh*. ^{1}H NMR of **4a**-*dh* (400 MHz, $CDCl_3$): δ 6.80 (d, 1H), 6.63 (d, 1H), 5.42 (dd, 1H), 3.49 (m, 1H), 2.52 (t, 2H), 1.57 (m, 2H), −13.02 (dd, hydride), −13.82 (d, J_{H-H} = 1 Hz, hydride). ^{2}D NMR of **4a**-*dh* (59 MHz, CH_2Cl_2): 3.67 (br s), deuterium incorporation at C(2).

Hydrogenation of 2a−c. Orange crystals of **2a** (100 mg, 0.106 mmol) were dissolved in 25 mL of CH_2Cl_2 and transferred to a Parr kinetic hydrogenator. The pressure vessel was sealed and flushed with hydrogen gas for 3 min. The hydrogenator was then placed in an oil bath at 75 °C, and the pressure was raised to 1000 psi. The reaction was allowed to proceed for 22 h. The vessel was allowed to cool, and the pressure was released to the atmosphere. The solvent was removed on a rotary evaporator, and the residue was chromatographed by TLC in hexane/CH_2Cl_2, ratio of 3:1. The faster moving band afforded **3a** (70 mg, 69% yield). The slower moving band afforded **2a** (4 mg, 5% yield); **3a**-d_2 was also prepared by the above method (75% yield).

Spectroscopic Data for Compound 3a-d_2. ^{1}H NMR of **3a**-d_2 (400 MHz, $CDCl_3$): δ 8.17 (d, H(2)), 7.17 (d, H(4)), 6.41 (t, (H3)), 2.72 (m, CH_2(5), CHD(7)), 1.72 (m, CH_2(6)), −13.73 (m, hydride), −13.95 (s, hydride). ^{2}D NMR of **3a**-d_2 (59 MHz, CH_2Cl_2): δ −13.78 (2 singlets partially resolved), 2.62 (br s).

X-ray Structure Determination of 2a, 3b, 5, and 6b. Crystals of **2a**, **3b**, **5**, and **6b** for X-ray examination were obtained from saturated solutions of each in hexane/dichloromethane solvent systems at −20 °C. Suitable crystals of each were mounted on glass fibers, placed in a goniometer head on the Enraf-Nonius CAD4 diffractometer, and centered optically. Unit-cell parameters and an orientation matrix for data collection were obtained by using the centering program in the CAD4 system. Details of the crystal data are given in Table 1. For each crystal, the actual scan range was calculated by scan width = scan range + 0.35 tan θ, and backgrounds were measured by using the moving-crystal moving-counter technique at the beginning and end of each scan. Two representative reflections were monitored every 2 h as a check on the instrument and crystal stability, and an additional two reflections were monitored periodically for crystal orientation control. Lorentz, polarization, and decay corrections were applied, as was an empirical absorption correction based on a series of Ψ scans, for each crystal. The weighting scheme used during refinement was $1/\sigma^2$, based on counting statistics.

Each of the structures was solved by the Patterson method using SHELXS-86,[18] which revealed the positions of the metal atoms. All other non-hydrogen atoms were found by successive difference Fourier syntheses. The expected hydride positions in each were calculated by using the program HYDEX,[10] hydrogen atoms were included in each structure and were placed in their expected chemical positions using the HFIX command in SHELXL-93.[19] The hydrides were given fixed positions and *U*'s, and other hydrogen atoms were included as riding atoms in the final least-squares refinements with *U*'s which were related to the atoms ridden upon. All other non-hydrogen atoms were refined anisotropically in **6b**, while in **5** and **2a**, only the osmium, oxygen, nitrogen, and ligand carbons were refined anisotropically, and in **3b**, only the osmium and oxygens could be refined anisotropically.

The ADP's of the carbon atoms in the phosphite ligand in **6b** were quite elongated, which indicated disorder or a large thermal effect. No attempt was made to resolve this behavior. Scattering factors were taken from Cromer and Waber.[20] Anomalous dispersion corrections were those of Cromer.[21] All data processing was carried out on a DEC 3000 AXP computer using the Open MolEN system of programs.[22] Structure solution and refinement and preparation of figures and tables for publication were carried out on PC's using SHELXS-86,[18] SHELXL-93,[19] and XP/PC[23] programs.

Acknowledgment. We gratefully acknowledge the National Science Foundation (Grant NO. CHE9625367, E. Rosenberg), the Consiglio Nazionale delle Ricerche (CNR, L. Milone), the Ministry of Education (L. Milone), the University of Montana (E. Rosenberg), the University of Turin (E. Rosenberg and L. Milone), and the CNR Programma di Scambi Internazionali (E. Rosenberg).

Supporting Information Available: Tables of atomic coordinates, anisotropic thermal parameters, and complete distances and angles for **2a**, **3b**, **5**, and **6b** (15 pages). Ordering information is given on any current masthead page.

OM970569H

(18) Sheldrick, G. M. *Acta Crystallogr.* **1990**, *A46*, 467.
(19) Sheldrick, G. M. *Program for Structure Refinement*; University of Göttingen: Göttingen, Germany, 1993.
(20) Cromer, D. T.; Waber, J. T. *International Tables for X-ray Crystallography;* Kynoch: Birmingham, 1974; Vol. 4, Table 2.2B.
(21) Cromer, D. T. *International Tables for X-ray Crystallography*; Kynoch: Birmingham, 1974; Vol. 4, Table 2.3.1.
(22) Fair, C. Kay. *MolEN. Structure Determination System;* Enraf-Nonius: Delft, The Netherlands, 1990.
(23) *XP/PC Molecular Graphics Software;* Siemens Analytical X-ray Instruments, Inc.: Madison, WI.